Invited Plenary Lecture given at the 17th International Conference on Nucleation and Atmospheric Aerosols, Galway Ireland, August 2007. Published in "Nucleation and Atmospheric Aerosols," Springer, Berlin, (2007) pp. 267-277.

Homogeneous Binary Nucleation Theory and the Structure of Binary Nanodroplets

Gerald Wilemski

Abstract The structure of a critical nucleus or a larger post-critical droplet refers to the spatial distributions of the different chemical species within the droplet. Structure directly affects the free energy of formation of droplets. This has a strong effect on the nucleation rate as well as on the rates of droplet growth and evaporation. Structure also affects how aerosol droplets interact with their environment, influencing phenomena such as heterogeneous chemistry, trace gas adsorbtion and uptake, and the radiative properties of larger droplets. This paper briefly reviews recent advances in understanding the structure of critical nuclei in highly nonideal binary systems. It then focuses on recent theoretical work to predict the structure of larger binary nanodroplets using density functional theory (DFT) and lattice Monte Carlo (MC) simulations of model aqueous-organic mixtures.

Keywords Homogeneous nucleation, binary nucleation, nanodroplets, clusters

Introduction

Evidence for multicomponent homogeneous nucleation of particles in the atmosphere is considerable and increasing.[1–3] Under the right conditions, these particles will continue to grow, passing through the several nanometer-size range until they become Aitken nuclei. With further growth, these particles may become cloud condensation nuclei. While these processes are broadly understood, many of the details are still hazy, and will depend on the local thermodynamic conditions and chemical composition of the atmosphere, among other factors. It is well-known that temperature and the partial pressures and chemical identities of the participating molecular species have a strong influence on particle nucleation and growth rates. These factors also strongly influence the structure of critical nuclei and of the larger post-critical droplets, and this paper will summarize some recent developments in this

Department of Physics and Cloud and Aerosol Sciences Laboratory, University of Missouri-Rolla, Rolla Missouri USA 65409-0640

C. D. O'Dowd and P. E. Wagner (eds.), *Nucleation and Atmospheric Aerosols*, 267–277.
doi: ; © Springer 2007

area. By structure, I mean the average spatial distributions of the various chemical species within the droplet. This notion is most useful for droplets containing many thousands down to several tens of molecules, and its utility rapidly diminishes with further decreases in cluster size. Hence, my considerations will not apply to the structure of small molecular clusters with fewer than, say, ~30 molecules. This review is not intended to be comprehensive, and it will concentrate mainly on my own studies on binary nanodroplets of 1–30 nm radius.

Small Critical Nuclei

For typical experimental conditions, binary critical nuclei generally contain 30–100 molecules. The role of structure in these cases is easiest to appreciate by considering the well-known effect of surface enrichment in alcohol–water systems. Alcohol molecules preferentially concentrate at the vapor–liquid interfaces of small droplets and bulk systems, lowering their interfacial tensions. In binary nucleation, this greatly reduces the work of forming the critical nucleus, thereby leading to the well-known mutual enhancement of nucleation.[4–7] Bulk thermodynamic models[8–10] of this phenomenon lead to unphysical results,[10] but progress has been made using phenomenological models for the surface composition.[11–13] In particular, the Laaksonen and Kulmala model[12] has been quite successful at describing structure in terms of compositional variables.[14,15] Models of this type provide only a simple characterization of the cluster structure. To obtain detailed spatial resolution, microscopic treatments based on statistical mechanics or molecular simulations are required.

Early microscopic treatments of surface enrichment in binary nucleation were made with density functional theory (DFT) for simple binary Lennard–Jones (LJ) clusters[16,17] and more complex models of amphiphiles.[18] More sophisticated DFT models of amphiphilic systems with LJ dimers and trimers have been used recently to demonstrate interesting lamellar structures in the critical nucleus, as well as the mutual enhancement of nucleation.[19,20]

The clearest demonstrations of surface enrichment are from computer simulations using molecular dynamics[21,22] (MD) or Monte Carlo[21,23] (MC) techniques, which produce computer-generated images of the clusters. Beyond this visualization capability, these techniques allow the full effect of cluster structure on the nucleation process to be studied quantitatively for quite realistic model systems. Recent innovations in MC sampling techniques by Chen et al.[23] and by McKenzie and Chen[24] now allow the construction of the free energy surface (FES) on which nucleation takes place for systems governed by complex and realistic intermolecular potentials. This capability permits detailed studies of nucleation pathways and mechanisms under conditions comparable to those studied experimentally. Recent studies[23, 24] of water/ethanol nucleation reproduced the mutual enhancement effect with results that were in excellent qualitative and reasonable quantitative accord with the experimental critical activities.[14]

Surface enrichment in the miscible water–alcohol systems is a clear manifestation of nonideal thermodynamic behavior.[25] Even more interesting structural effects arise when nonideality is extreme, i.e., in partially miscible and nearly immiscible systems. Using classical nucleation theory (CNT), Ray et al.[26] found that the FES of a partially miscible system could have double saddle points (DSP), i.e., two types of mixed critical nuclei may occur for the same vapor state. Although CNT is useful in studying how the DSP affects the kinetics of nucleation,[26,27] it does not reveal the structures of the critical nuclei. In a notable MC/MD study on small binary LJ clusters at low temperatures, Clarke et al.[21] identified numerous different cluster structures that could arise depending on the relative strengths of the different LJ energy parameters. Among the types found were well-mixed (WM) droplets, surface-enriched droplets, and nonspherical, phase-separated droplets. Although these insights into the energetics of cluster structure are valuable, they are less useful from a nucleation perspective since it is not clear when or if these structures may occur as critical nuclei. A step in this direction was provided by Talanquer and Oxtoby,[28] who used DFT in the square-gradient approximation to study binary nucleation of partially miscible LJ systems. In addition to finding DSP behavior, they also found nonspherical, phase-separated droplets, similar to those of Clarke et al.,[21] that appeared to afford an alternative nucleation pathway. Subsequent MC simulations by ten Wolde and Frenkel[29] and more sophisticated DFT calculations by Napari and Laaksonen[30] for binary LJ clusters showed that the phase-separated clusters were not critical nuclei but corresponded to local maxima on the FES, and hence were not important for nucleation. Note that the work of Talanquer and Oxtoby,[28] ten Wolde and Frenkel,[29] and Napari and Laaksonen[30] was conducted at a single, relatively high temperature, roughly twice as high as that used in the earlier study of Clarke et al.[21] Thus, while nonspherical, phase-separated LJ droplets may not serve as critical nuclei at temperatures near the triple point, this possibility remains an open question at lower temperatures.

Recent work by McKenzie and Chen[24] bears on this issue. One of the systems they studied, nonane–ethanol, exhibits quite unusual behavior at $T = 230$K, the low temperature used in the experiments of Viisanen et al.[31] For a small range of vapor conditions, the saddle region on the FES was broad and flat, rendering ambiguous the notion of a single critical nucleus with a well-defined composition. This feature persisted at 300K and, to a lesser extent, at 360K as well. They analyzed a subset of clusters at 230K with similar numbers (20 ± 2) of *n*-nonane and ethanol molecules. These compositions lie on the flat part of the saddle. They found that these clusters had a structure resembling that of the nonspherical, phase-separated LJ droplets studied by Clarke et al.[21] and Talanquer and Oxtoby.[28] They did not discuss the structure of the high temperature critical nuclei. Thus, in a system decidedly different from a binary LJ mixture, there seems to be strong evidence for the role of highly asymmetric critical nuclei at low temperatures. As I will discuss in the next section, the key to the stability of much larger phase-separated droplets also appears to be low temperature.

Large Nanodroplets

Recent experimental and theoretical efforts to understand the structure of aqueous-organic nanodroplets are largely motivated by the atmospheric importance of these systems.[32,33] Typically, the organic species are only sparingly soluble in water, and the bulk mixtures have miscibility gaps between coexisting water-rich and organic-rich phases whose compositions depend on the nature of the organic species. This phase behavior leads one to anticipate a nonuniform distribution of organic matter in water-rich aqueous-organic aerosol droplets, e.g., in the form of an aqueous core surrounded by a shell of organic material.[34] Indeed, there is experimental support for such core-shell (CS) structures from surface analyses of atmospheric aerosol particles[35] and even more evidence from small-angle neutron scattering measurements on nanodroplets containing the partially miscible species water and *n*-butanol.[36] Two recent theoretical studies explore the structures of aqueous-organic nanodroplets that can occur under various conditions. Both DFT[37] and lattice MC[38] (LMC) techniques were used to treat binary fluid models that emulated the characteristics of partially miscible aqueous-organic systems.

The DFT model of Li and Wilemski[37] is a binary mixture of hard spheres with attractive Yukawa forces. This approach is an extension to spherical droplets of Sullivan's theory[39] of interfaces in the binary van der Waals fluid. It generalizes the work of Oxtoby and Evans[40] for unary systems and is closely related to the DFT of Zeng and Oxtoby[16] for nucleation in binary fluids. In these theories, the grand potential is a functional of the species densities. The nature of the functional determines the complexity of the resulting Euler–Lagrange equations that must be solved to find the equilibrium droplet-density profiles. The earliest and simplest functionals[16,39] employ the random phase and local density approximations and produce integral Euler–Lagrange equations of the form

$$\mu_i = \mu_{ih}[\rho_1(\mathbf{r}), \rho_2(\mathbf{r})] + \sum_{j=1}^{2} \int d\mathbf{r}' \phi_{ij}\left(|\mathbf{r} - \mathbf{r}'|\right) \rho_j(\mathbf{r}'), \tag{1}$$

where μ_i is the chemical potential of the ith component in the system, μ_{ih} is the local chemical potential of species i in a hard sphere fluid mixture,[41] $\rho_i(\mathbf{r})$ is the average number density of species i at point $\mathbf{r}$, and ϕ_{ij} is the attractive part of the pair potential between molecules of species i and species j. Although more sophisticated models of amphiphilic systems have been developed,[18–20] we adopted the simpler, pseudopotential approach of Sullivan[39] by retaining Eq. (1) and choosing ϕ_{ij} as the Yukawa potential

$$\phi_{ij}(r) = -\alpha_{ij}\lambda^3 \exp(-\lambda r)/(4\pi\lambda r). \tag{2}$$

Here, α_{ij} controls the strength of the attractive intermolecular potential, and λ is an inverse range parameter that is assumed to be the same for all pair interactions. For this choice of ϕ_{ij}, acting with ∇^2 on the coupled integral Euler–Lagrange Eq. (1), produces two coupled differential equations that resemble nonlinear diffusion equations,

$$^{2}\mu_{ih} = \lambda^{2}(\mu_{ih}(\rho_1,\rho_2) - \mu_i - \sum_{j=1}^{2}\alpha_{ij}\rho_j). \quad (3)$$

The cross interaction term is assumed to obey the so-called Bertholet (geometric mean) mixing rule, $\alpha_{12} = \sqrt{\alpha_{11}+\alpha_{22}}$. This leaves five independent parameters (λ, α_{11}, α_{22}, and two hard sphere diameters) whose values are chosen to fit the density of pure water and the surface tensions and vapor pressures of both pure fluids at 250K.

The mean-field van der Waals equation of state for this pseudo water–pentanol mixture captures most of the features of real water–pentanol mixtures. As illustrated in the published phase diagram,[37] the model correctly predicts bulk liquid–liquid phase separation at small values of $x_{p\text{-Pentanol}}$, the *p*-pentanol mole fraction.[42] The model bulk surface tension is also realistic: there is a steep drop at low values of $x_{p\text{-Pentanol}}$ in the water-rich (L1) phase and a slow variation in the alcohol-rich (L2) phase.[37]

Two principal types of droplet structures were evident in the extensive DFT calculations. These are illustrated in Figure 1 for two moderately large nanodroplets (radius ~ 4–5 nm). In the WM droplet structure, Figure 1(a), the density profiles are fairly flat throughout most of the droplet. As the vapor–liquid interface is approached, the *p*-water density tends to decay more quickly leaving a *p*-pentanol-rich coating on the droplet surface. These structures resemble the bulk L2-liquid–vapor interface. Similarly the CS structure in Figure 1(b) resembles the bulk L1-vapor interface. Furthermore, the CS structure is consistent with that inferred from the recent SANS measurements of Wyslouzil et al.[36] the core is very rich in *p*-water, and the *p*-pentanol concentration remains small until the vapor–liquid interface is reached. In the interfacial region, the *p*-water density falls rapidly, while the *p*-pentanol density profile is a roughly Gaussian shaped adsorbed layer. As shown elsewhere,[37] the thickness and density of this adsorbed layer varies with the *p*-pentanol vapor concentration.

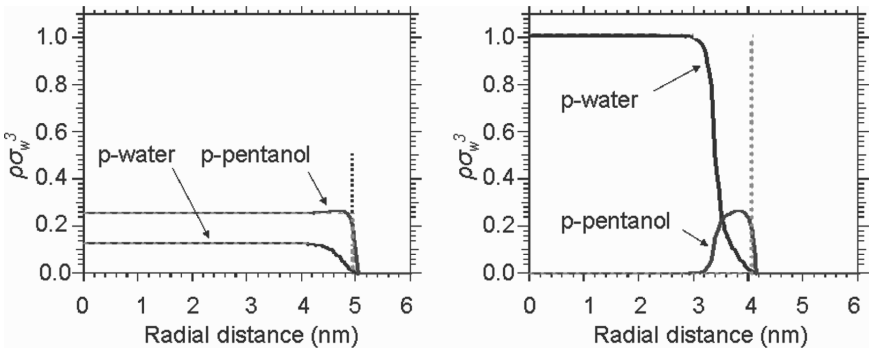

Figure 1 Density profiles of critical droplets at vapor state activities, $a_P = 1.002$, $a_W = 1.178$ ($a_i = p_i/p_i^0$, where p_i and p_i^0 are the actual and equilibrium vapor pressures of species *i*, respectively); the mol percentage of *p*-pentanol is 2.64% in the bulk gas phase. The droplet size is well described by the vertical dashed line, which is the Gibbs dividing surface of Buff.[43] (a) Left: a well-mixed structure. (b) Right: a core-shell structure. Note that both structures occur at the same vapor state

Despite the relative simplicity of our model, the interfacial density profiles are quite similar to those found in MC simulations of bulk butanol–water interfaces with realistic intermolecular potentials.[44] The similarity of the two sets of results supports the utility and efficacy of this semiempirical model in these types of investigations.

Figure 2 is a phase diagram for the different droplet structures illustrated in Figure 1 calculated using DFT.[37] The coordinates of the diagram are the vapor phase activities of the *p*-water and *p*-pentanol species, as defined in the Figure 1 caption. The theory predicts that there is a bistructural region where both types of droplet structures may occur simultaneously at the same vapor state. Binary CNT[45] also predicts a bi-structural region (shown in Ref. 37) whose lower boundary agrees fairly well with the DFT results, although there is a growing discrepancy as the water activity increases. In contrast there is a major discrepancy in the upper boundary: the coexistence region predicted by CNT is much broader than that predicted by DFT.[37] These discrepancies with CNT highlight the need for a non-classical theory, such as DFT. Note that the droplet structures shown in Figure 1 are calculated for the same vapor phase state in the bistructural region of Figure 2. The bistructural region of the phase diagram is consistent with the DSP behavior found in earlier studies of vapor phase nucleation using CNT[26,27] and DFT,[28] as discussed earlier.

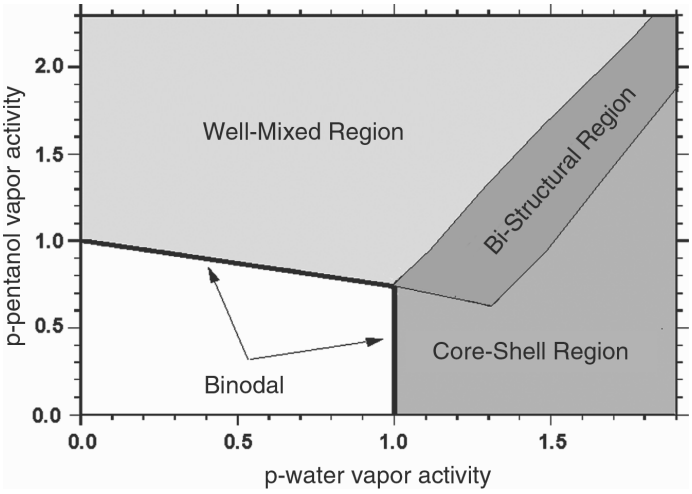

Figure 2 A structural phase diagram for aerosol nanodroplets. The heavy solid lines are the vapor binodal compositions. The shaded regions are supersaturated vapor states. In the bistructural region, both types of droplet structures can occur at the same vapor state, although with different free energies. In the upper region, only well-mixed droplets, as shown in Figure 1a, are found. In the lower region, only core-shell droplet structures, as shown in Figure 1b, are found. Droplet radii along the upper and right boundaries of this diagram are roughly 1–2 nm; the largest droplets studied, with 30 nm radii, are found close to the binodal lines

Phase diagrams of the sort shown in Figure 2 may play an important role in future models of the radiative effects of atmospheric aerosols, because the internal structure of a particle directly affects its radiative properties and strongly influences the size and number density of droplets that may form in clouds. The latter, so-called indirect effect, has a major influence on the earth's albedo and hydrological cycles, but is still poorly quantified.[33] Progress on this problem will depend in part on a better understanding of aerosol-particle structure. For example, the bistructural region in Figure 2 implies that aerosol structural transitions will exhibit hysteresis in the same way that salt-containing aerosol particles do when undergoing deliquescence and efflorescence.[46,47] Finally, it should be noted that the phase diagram of Figure 2 may be incomplete since the theory underlying it considered only spherically symmetric droplet structures.

Recently, Ning and Wilemski have begun to address the effect of temperature on nanodroplet structure with MC simulations of model aqueous-organic nanodroplets containing roughly 4,000 particles.[37] They used a simple fcc lattice model with nearest neighbor interactions. Their approach generalizes the earlier LMC work of Cordeiro and Pakula[48] who simulated unary droplets. For the results shown here, a 32,000 site fcc lattice was partially filled by 1,400 type 1 and 3,400 type 2 beads. The beads interact repulsively with vacant sites, i.e., E_1 and $E_2 > 0$, and the interaction between different bead types E_3 may be repulsive (>0) or attractive (<0), depending on the desired type of mixture behavior. The energy scale is set by taking the type 1 bead-vacancy interaction to be unity, $E_1 = 1$. Simulation temperatures are given in terms of kT scaled by E_1. For a system of pure type 1 beads, the estimates of Cordeiro and Pakula[48] for the critical temperature and the "triple point" temperature are $kT_c = 5.3$ and $kT_t = 2.8$, respectively. The binary droplet simulations were made for $kT < 2.75$, and are, thus, at temperatures subcooled with respect to the pure type 1 "liquid." The basic MC move is the interchange of a randomly chosen bead with a randomly selected nearest neighbor. The usual Metropolis acceptance rule is then applied. One MC step equals N exchange attempts, where N is the total number of beads on the lattice.

By varying E_2 and E_3, various types of droplet structures can be realized. These include WM, surface-enriched, CS, and a nonspherical, phase-separated structure, termed a Russian doll (RD). Snapshots of the latter two structures are shown in Figure 3. The RD structure is similar to that found by Clarke et al.[21] and Talanquer and Oxtoby[28] for much smaller droplets. It occurs at low temperatures for a highly unfavorable cross interaction, $E_3 = 0.8$. A remarkable feature of this structure is that it gradually converts into a CS structure as the temperature increases. This can be understood as a wetting transition that occurs at a relatively well-defined temperature (for the droplet size studied). Young's equation[49] provides a simple macroscopic interpretation of the transition in the idealized case of a nondeformable type 1 substrate coated by type 2 fluid. The RD structure corresponds to the imperfect wetting by type 2 fluid of the type 1 substrate with a nonzero contact angle θ. Young's equation for the balance of interfacial tensions then reads, $\gamma_{bv} = \gamma_{rb} + \gamma_{rv} \cos \theta$, from which it follows that there is a surface free energy penalty associated with spreading fluid 2 over substrate 1 ($\gamma_{bv} < \gamma_{rb} + \gamma_{rv}$). As T increases, the interfacial

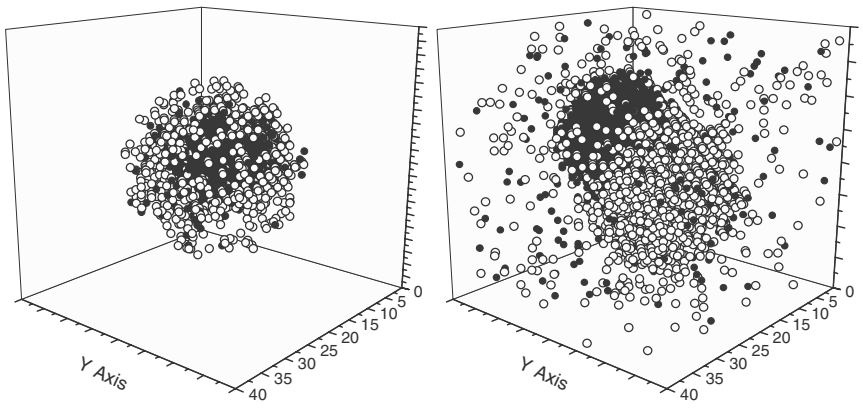

Figure 3 Snapshots of binary lattice droplet structures formed for $E_2 = 2/3$ and $E_3 = 0.8$: (**Left**) Core-shell structure at $kT = 2.6$ with vapor removed. (**Right**) Russian doll structure at $kT = 2.0$ showing vapor. Type 1 beads (water-like) are shown in black, while type 2 beads (organic-like) are open circles

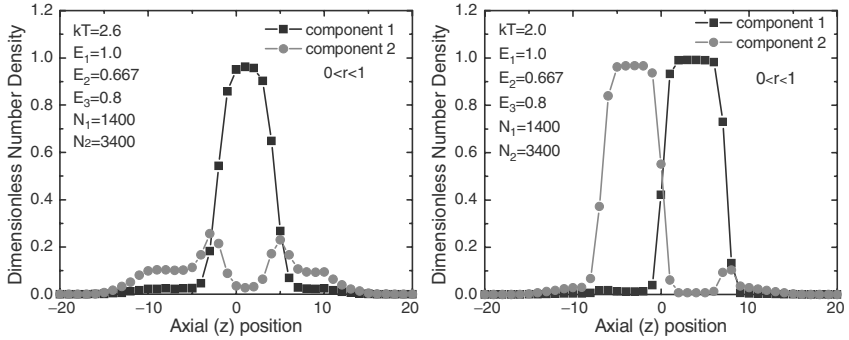

Figure 4 Axial density profiles for core-shell and Russian doll structures averaged over 10^7 Monte Carlo steps. The density is the fraction of sites within a small region occupied by beads of type 1 or type 2. Note that the CS droplet profile (**left**) at $kT = 2.6$ is slightly asymmetric because of dewetting. The RD droplet profile (**right**) at $kT = 2.0$ is highly asymmetric due to dewetting and phase separation

tensions decrease in such a way as to reach the condition $\theta = 0$. Antonow's rule for perfect wetting is then satisfied, $\gamma_{bv} = \gamma_{rb} + \gamma_{rv}$, the free energy penalty is absent, and fluid 2 spreads spontaneously over the substrate 1 resulting in the CS droplet structure.

The transition is reversible in the sense that changing the temperature in either direction causes a change in structure to occur without apparent hysteresis. The RD structures are stable over runs as long as 10^7 MC time steps, and statistically similar results were found from several different initial conditions. The radial density profiles for the CS droplet are similar to those of Figure 1b.

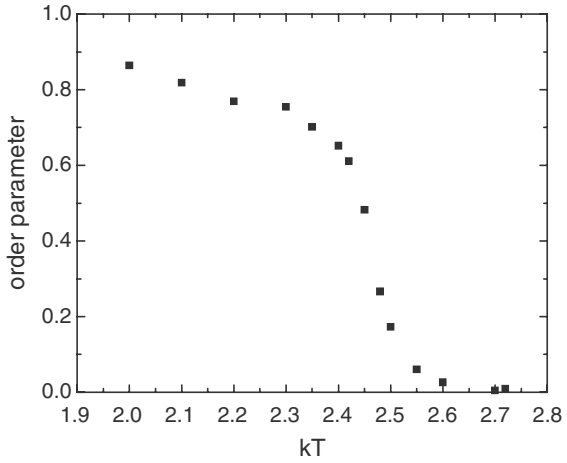

Figure 5 The microscopic order parameter η for the wetting transition is plotted versus T; η is a simple measure of the asymmetry in the type 2 bead number density profile with respect to $z = 0$

Density profiles along an internal z-axis for the CS and RD structures are illustrated in Figure 4. This z-axis is a line passing through the centers of "mass" of the type 1 and type 2 beads with $z = 0$ at the overall center of mass. The wetting/dewetting transition may be characterized by a microscopic order parameter η, defined here as the difference in the peak heights of the two maxima in the type 2 bead axial density profile. A plot of this order parameter versus T is shown in Figure 5. For CS structures η is quite small, but not zero due to fluctuations. Below the dewetting transition temperature, η increases monotonically as the RD structure grows increasingly anisotropic.

Indirect support for imperfect wetting of organics on water droplets comes from recent droplet growth measurements by Peeters et al.[50] in ternary water–nonane–methane mixtures at high pressure and low temperature (242 and 247K). In summary, the key to the stability of the RD droplets appears to be low temperature. Given the range of temperatures in the atmosphere and the ubiquity of aqueous-organic droplets, structural transitions of this sort could be a common occurrence there.

References

1. Spracklen, D.V., Carslaw, K.S., Kulmala, M., Kerminen, V.-M., Mann, G.W., and Sihto, S.-L., The contribution of boundary layer nucleation events to total particle concentrations on regional and global scales, *Atmos. Chem. Phys*., **6**, 5631–5648 (2006).
2. O'Dowd, C.D., and Hoffman, T., Coastal new particle formation: a review of the current state-of-the-art, *Environ. Chem*., **2**, 245–255 (2005).

3. Dunn, M.J., Jimenez, J.L., Baumgardner, D., Castro, T., McMurry, P.H., and Smith, J.N., Measurements of Mexico City nanoparticle size distributions: observations of new particle formation and growth, *Geophys. Res. Lett*., **33**, L15802/1–4, (2006).
4. Schmitt, J.L., Whitten, J., Adams, G.W., and Zalabsky, R.A., Binary nucleation of ethanol and water, *J. Chem. Phys*., **92**, 3693–3699 (1990).
5. Strey, R., Viisanen, Y., and Wagner, P.E., Measurement of the molecular content of binary nuclei. III. Use of the nucleation rate surfaces for the water-*n*-alcohol series, *J.Chem.Phys*., **103**, 4333–4345 (1995).
6. Rodemann, T. and Peters, F., Experimental investigation of binary nucleation rates of water-*n*-propanol and water-*n*-butanol vapors by means of a pex-tube, *J.Chem.Phys*., **105**, 5168–5176 (1996).
7. Wyslouzil, B.E., Heath, C.H., Cheung, J.L., and Wilemski, G., Binary condensation in a supersonic nozzle, *J.Chem.Phys*., **113**, 7317–7329 (2000).
8. Flood, H., Formation of droplets in mixtures of the vapors of ethyl alcohol and water, *Z. Physik. Chem. A*, **170**, 286–294 (1934).
9. Neumann, K. and Döring, W., Droplet formation in supersaturated mixtures of the vapors of two completely miscible liquids, *Z. Physik. Chem. A*, **186**, 203–226 (1940).
10. Wilemski, G., Revised classical binary nucleation theory for aqueous alcohol and acetone vapors, *J. Phys. Chem*., **91**, 2492–2498 (1987).
11. Flageollet-Daniel, C., Garnier, J.P., and Mirabel, P., Microscopic surface tension and binary nucleation, *J. Chem. Phys*., **78**, 2600–2606 (1983).
12. Laaksonen, A. and Kulmala, M., An explicit cluster model for binary nuclei in water-alcohol systems, *J. Chem. Phys*., **95**, 6745–6748 (1991).
13. Laaksonen, A., Nucleation of binary water-*n*-alcohol vapors, *J. Chem. Phys*., **97**, 1983–1989 (1992).
14. Viisanen, Y., Strey, R., Laaksonen, A., and Kulmala, M., Measurement of the molecular content of binary nuclei. II. Use of the nucleation rate surface for water-ethanol, *J. Chem. Phys*., **100**, 6062–6072, (1994).
15. Salonen, M., Napari, I., and Laaksonen, A., Modeling of critical cluster structure in surface active systems, in: *Nucleation and Atmospheric Aerosols, 2004*, edited by M. Kasahara and M. Kulmala, Kyoto: Kyoto University Press (2004), pp. 277–280.
16. Zeng, X.C. and Oxtoby, D.W., Binary homogeneous nucleation theory for the gas-liquid transition: A nonclassical approach, *J. Chem. Phys*., **95**, 5940–5947 (1991).
17. Laaksonen, A. and Oxtoby, D.W., Gas-liquid nucleation of nonideal binary mixtures. I. A density functional study, *J. Chem. Phys*., **102**, 5803–5810 (1995).
18. Talanquer, V. and Oxtoby, D.W., Nucleation in the presence of an amphiphile: a density functional approach, *J. Chem. Phys*., **106**, 3673–3680 (1997).
19. Napari, I. and Laaksonen, A., Surfactant effects and an order-disorder transition in binary gas-liquid nucleation, *Phys. Rev. Lett*., **84**, 2184–2187 (2000).
20. Napari, I., Laaksonen, A., and Strey, R., Density-functional studies of amphiphilic binary mixtures. II. Gas-liquid nucleation, *J. Chem. Phys*., **113**, 4480–4487 (2000).
21. Clarke, A.S., Kapral, R., and Patey, G.N., Structure of two-component clusters, *J. Chem. Phys*., **101**, 2432–2445 (1994).
22. Tarek, M. and Klein, M.L., Molecular dynamics study of two-component systems: The shape and surface structure of water/ethanol droplets, *J. Phys. Chem. A*, **101**, 8639–8642 (1997).
23. Chen, B., Siepmann, J.I., and Klein, M.L., Simulating the nucleation of water/ethanol and water/*n*-nonane mixtures: mutual enhancement and two-pathway mechanism, *J. Am. Chem. Soc*., **125**, 3113–3118 (2003).
24. McKenzie, M.E. and Chen, B., Unravelling the peculiar nucleation mechanisms for non-ideal binary mixtures with atomistic simulations, *J. Phys. Chem. B*, **110**, 3511–3516 (2006).
25. Osborne, M.J., and Lacks, D.J., Surface segregation in liquid mixtures with strong interspecies attraction, *Phys. Rev. E*, **70**, 010501(R)/1–4, (2004).
26. Ray, A.K., Chalam, M., and Peters, L.K., Homogeneous nucleation of binary vapors partially miscible in liquid state, *J. Chem. Phys*., **85**, 2161–2168 (1986).

27. Wyslouzil, B.E. and Chen, S., Binary nucleation kinetics. 6. Partially miscible systems, *J. Phys. Chem. B*, **105**, 11566–11573 (2001).
28. Talanquer, V. and Oxtoby, D.W., Critical clusters in binary mixtures: a density functional approach, *J. Chem. Phys*., **104**, 1993–1999 (1996).
29. ten Wolde, P.R. and Frenkel, D., Numerical study of gas-liquid nucleation in partially miscible binary mixtures, *J. Chem. Phys*., **109**, 9919–9927 (1998).
30. Napari, I. and Laaksonen, A., Gas-liquid nucleation in partially miscible systems: Free-energy surfaces and structures of nuclei from density functional calculations, *J. Chem. Phys*., **111**, 5485–5490 (1999).
31. Viisanen, Y., Wagner, P.E., and Strey, R., Measurement of the molecular content of binary nuclei. IV. Use of the nucleation rate surfaces for the *n*-nonane-*n*-alcohol series, *J.Chem. Phys*., **108**, 4257–4266 (1998).
32. Charlson, R.J., Seinfeld, J.H, Nenes, A., Kulmala M., Laaksonen, A., and Facchini, M.C., Atmospheric science. Reshaping the theory of cloud formation, *Science*, **292**, 2025–2026 (2001).
33. Schwartz, S.E., Aerosols, clouds, and climate change, in: *Nucleation and Atmospheric Aerosols, 2004*, edited by M. Kasahara and M. Kulmala, Kyoto: Kyoto University Press , pp. 323–338 (2004).
34. Ellison, G.B., Tuck, A.F., and Vaida, V., Atmospheric processing of organic aerosols, *J. Geophys. Res. Atmos*., **104**, 11633–11641 (1999).
35. Tervahattu, H., Juhanoja, J., Vaida, V., Tuck, A.F., Niemi, J.V., Kupiainen, K., Kulmala, M., and Vehkamaki, H, Fatty acids on continental sulfate aerosol particles, *J. Geophys. Res., Atmos*., **110**, D06207/1–9 (2005).
36. Wyslouzil, B.E., Wilemski, G., Strey, R., Heath, C.H., and Dieregsweiler, U., Experimental evidence for internal structure in aqueous-organic nanodroplets, *Phys. Chem. Chem. Phys*., **8**, 54–57 (2006).
37. Li, J.S. and Wilemski, G., A structural phase diagram for model aqueous organic nanodroplets, *Phys. Chem. Chem. Phys*., **8**, 1266–1270 (2006).
38. Ning, H.X. and Wilemski, G., Structure in binary nanodroplets, presented at the 2006 APS March Meeting, Baltimore, MD, 16 March 2006; *Bull. Am. Phys. Soc*., **51**, 1227 (2006).
39. Sullivan, D.E., Interfacial density profiles of a binary van der Waals fluid, *J. Chem. Phys*., **77**, 2632–2638 (1982).
40. Oxtoby, D.W. and Evans, R. Nonclassical nucleation theory for the gas-liquid transition, *J. Chem. Phys*., **89**, 7521–7530 (1988).
41. Mansoori, G.A., Carnahan, N.F., Starling, K.E., and Leland, T.W., Equilibrium thermodynamic properties of mixture of hard spheres, *J. Chem. Phys*., **54**, 1523–1525 (1971).
42. Gross, J. and Sadowski, G., Application of the perturbed-chain SAFT equation of state to associating systems, *Ind. Eng. Chem. Res*., **41**, 5510–5515 (2002).
43. Buff, F.P., Some considerations of surface tension, *Z. Elektrochem*., **56**, 311–313 (1952).
44. Chen, B., Siepmann, J.I., and Klein, M.L., Vapor-liquid interfacial properties of mutually saturated water/1-butanol solutions, *J. Am. Chem. Soc*., **124**, 12232–12237 (2002).
45. Nishioka, K. and Kusaka, I., Thermodynamic formulas of liquid-phase nucleation from vapor in multi-component systems, *J. Chem. Phys*., **96**, 5370–5376 (1992).
46. Randles, C.A., Russell, L.M., and Ramaswamy, V., Hygroscopic and optical properties of organic sea salt aerosol and consequences for climate forcing, *Geophys. Res. Lett*., **31**, L16108/1–4, (2004).
47. Tang, I., Thermodynamic and optical properties of mixed-salt aerosols of atmospheric importance, *J. Geophys. Res*., **102**, 1883–1893 (1997).
48. Cordeiro, R. M., and Pakula, T., Behavior of evaporating droplets at nonsoluble and soluble surfaces: Modeling with molecular resolution, *J. Phys. Chem. B*, **109**, 4152–4161 (2005).
49. Rowlinson, J.S. and Widom, B., *Molecular Theory of Capillarity*, Oxford: Oxford University Press , p. 9 (1982).
50. Peeters, P., Pieterse, G., Hrubý, J., and van Dongen, M.E.H., Multi-component droplet growth. I. Experiments with supersaturated *n*-nonane vapor and water vapor in methane, *Phys. Fluids*, **16**, 2567–2574 (2004).